12th IEA Heat Pump Conference 2017

Absorption of CO_2-NH_3-H_2O mixture in mini-channel heat exchangers

Liang Shi[a], Vilborg Gudjonsdottir[a]*, Carlos A. Infante Ferreira[a], Glenn Rexwinkel[b], Anton A. Kiss[c]

[a]Process and Energy Laboratory, Delft University of Technology, Leeghwaterstraat 39, 2628 CB, Delft, The Netherlands;
[b]Frames, Eikenlaan 237,2404 BP Alphen aan den Rijn, The Netherlands;
[c]AkzoNobel – Research, Development & Innovation, Process Technology SRG, Zutphenseweg 10, 7418 AJ Deventer, The Netherlands

Abstract

Compression resorption heat pumps (CRHP) are a promising option to upgrade waste heat from industry. Alternative working fluids can further improve the efficiency of CRHP. The ternary mixture NH_3-CO_2-H_2O has been identified as a promising working fluid for CRHP and has the potential to further enhance the coefficient of performance (COP) of the cycle compared to the traditionally used ammonia water mixture. So far the studies on the NH_3-CO_2-H_2O mixture have focused mainly on carbon capture applications. But the desired operating conditions are different than for CRHP applications, e.g. the NH_3 concentration. Additionally the absorption process with the mixture in tubular absorbers has not yet been reported. The focus of this study is therefore to investigate experimentally the absorption process of a CRHP with this ternary mixture. To reach this goal a model is developed for ammonia-water that takes into account the kinetics and mass transfer during the absorption process. To validate the model, experiments were performed for an absorption process in a mini channel heat exchanger with NH_3 concentration of 35 wt%. The results show a good match between the model and the experiments. Additionally CO_2 has been added to the solution and the experimental performance was compared with the experimental performance of the NH_3-H_2O mixture. A concentration of 2 wt% CO_2 resulted in a performance increase of up to 5% however the working fluid flow became limited by pumping instabilities.

Selection and/or peer-review under responsibility of the organizers of the12th IEA Heat Pump Conference 2017.

Keywords: heat pumps, NH_3-CO_2-H_2O mixture, NH_3-H_2O mixture, waste heat recovery, absorption, mini-channel heat exchangers

Nomenclature

A	area	m^2	*Greek symbols*		
c_p	heat capacity	$Jkg^{-1}K^{-1}$	α	heat transfer coefficient	$Wm^{-2}K^{-1}$

d	diameter	m	ϕ	heat flux	Wm^{-2}
F	mass transfer coefficient	$molm^{-2}s^{-1}$	ρ	density	kgm^{-3}
f	friction factor	-	λ	thermal conductivity	$Wm^{-1}K^{-1}$
G	mass flux	$kgm^{-2}s^{-1}$			
h	enthalpy	Jkg^{-1}	*Subscripts*		
$\tilde{h}$	partial enthalpy	Jkg^{-1}	*cw*	cooling water	
J	molar flux	$molm^{-2}s^{-1}$	*H*	hydraulic	
L	length	m	*i*	interface	
M	molar mass	$kgmol^{-1}$	*in*	inlet	
$\dot{m}$	mass flow	kgs^{-1}	*l*	liquid	
P	pressure	bar	*out*	outlet	
Q	heat flow	W	*s*	shell	
q	quality	-	*t*	tube	
Re	Reynolds number	-	*ti*	inner tube	
T	temperature	°C	*to*	outer tube	
u	velocity	ms^{-1}	*tp*	two-phase	
x	molar concentration	$molmol^{-1}$	*v*	vapor	
y	axial coordinate	m			
z	molar flux ratio	-			

1. Introduction

Industry contributes to a great part of the total energy consumption. In 2014, 30% of the total final energy consumption originated from the industry in the Netherlands [1]. This large share of energy consumption by industry indicates that developing technologies to increase the total efficiency of industrial processes has a great potential to save energy. Heat pump technology is one of the best options to recover energy in many industrial processes. Take cooling water as an example, a large amount of low grade waste heat is available as water from cooling towers with temperatures in the range of 45-60°C [2]. A previous study by van de Bor et al. [2] indicated that compression-resorption heat pumps (CRHP) can be integrated with industrial processes to recover heat and provide a higher efficiency compared to conventional vapor-compression heat pumps (VCHP). Similar to the vapor absorption cycle, the most common working pair used in CRHP cycle is the binary mixture ammonia-water. Ammonia-water mixture shows plenty of advantages: non-isothermal phase transition of the mixture at constant pressure in heat exchangers ensures higher coefficient of performance (COP) than pure working fluid for VCHP; the mixture can be operated at relatively low pressures to achieve high temperature; CRHP cycle can be designed to match the temperature glide of the industrial flow that has to be heated using the temperature glide in the resorber [3]. The CO_2-NH_3-H_2O mixture has been identified as a possible working fluid for CRHP, and a preliminary study suggests that it has better performance than ammonia-water [4]. Resorbers are important components in CRHP cycle and comparable to condensers in VCHP cycles. To evaluate the COP of the CRHP cycle, it is necessary to study the performance of the absorption process in resorbers in detail. Van Leeuwen [5] experimentally investigated absorption and desorption of ammonia-water mixtures in a tube-in-tube mini-channel heat exchanger and built a model to simulate these processes. The calculation method proposed by Fernandez-Seara et al. [6] served as a basis for the model. The study concludes that mini-channel heat exchangers provide a considerably higher overall heat transfer coefficient than conventional heat exchangers. Rijpkema [7] further developed a model following the

approach by van Leeuwen [5] to predict the performance of an ammonia-water mixture in a mini-channel, and the influence of the surface tension was investigated. The results show that modeling of surface tension has little effect on the absorption side, while on the desorption side it has significant effect. The current work performs experiments in a mini-channel heat exchanger using both ammonia-water binary mixture and CO_2-NH_3-H_2O ternary mixture to study the absorption process of a CRHP cycle. A corresponding mathematical model is developed to simulate the absorption process of ammonia-water mixture, while experimental data are used to validate the proposed model.

2. Experimental Setup

Fig. 1 shows the scheme of the experimental setup. The ammonia-water binary mixture or CO_2-NH_3-H_2O ternary mixture is fed from top to bottom on the tube side of the multi-tube mini-channel heat exchanger. The mini-channel heat exchanger acts as the resorber of a CRHP cycle and is the main test section of the experimental setup. The two cycles connected to the mini-channel heat exchanger are installed to ensure the inlet conditions of the mini-channel are as expected. The cycle on the right hand side in Fig. 1 represents the mixture absorption cycle. The pump compensates the pressure drop along the cycle and drives the mixture to flow through the system. A flow meter is installed after the pump to measure the flow rate of the cycle. After passing through the flow meter, the fluid mixture is heated up by a tube-in-tube heat exchanger of which the hot side is filled with silicon oil flowing through a thermostatic bath. Extra heating is provided by an electric tracing coil to keep the temperature at the inlet of the absorber stable. The fluid mixture changes its phase from vapor to liquid in the tube side of the mini-channel by releasing heat to the water on the shell side. A plate heat exchanger is installed after the mini-channel for further cooling of the fluid. Cooling water from a cooling tower is used to sub-cool the liquid before entering the pump. Mass flow of the cooling water passing through the plate heat exchanger is always set at the maximum flow rate to ensure the working fluid is sufficiently sub-cooled before entering the pump. The setup of the cycle on the left hand side is identical to the absorption cycle on the right hand side.

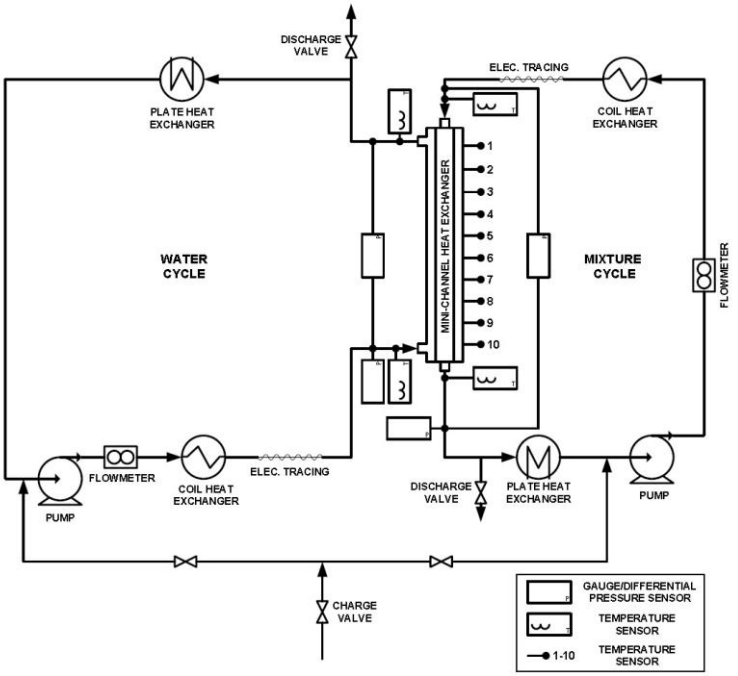

Fig. 1. Schematic diagram of experimental setup

Two parameters can be controlled on each side of the setup during the experiments: the mass flow of the cycle and the temperature at the inlet of the test section. Fluid temperature entering the absorber can be controlled by the thermostatic bath behind the flow meter and/or the tracing coil around the pipe before entering the mini-channel heat exchanger. The flow meters after the pumps are used to control the mass flow on both sides, they also give back the values of the temperature and the density of the fluid. Pressure sensors are installed at the inlets of the mini-channel heat exchanger to measure the gauge pressure and differential pressure sensors measure the pressure difference between in- and outlets of the absorber. Additionally 10 temperature sensors are averagely located on the outside of the shell of the mini-channel heat exchanger to investigate the temperature profile along the heat exchanger. The dimensions of the mini-channel heat exchanger are listed in Table 1. Design details can be found in Nefs et al. [8]. The accuracies of the different sensors are listed in Table 2.

Table 1. Main dimensions of the mini-channel heat exchanger

Parameter	Unit	Value
Number of tubes	-	116
Total length of heat exchanger section	mm	800
Inner diameter of the tube	mm	0.5
Outer diameter of the tube	mm	1.0
Inner diameter of the shell	mm	21
Outer diameter of the shell	mm	25

Table 2.Accuracy of the different sensors

Sensor	Type	Range	Accuracy	Unit
Temperature sensor	PT-100, Type B	-50...+200	±(0.3+0.005T)	°C
Mass flow sensor	mini Cori-Flow, M14	+0...+20	±0.04	kg/hr
Density sensor	mini Cori-Flow, M14	not given	±5	kg/m^3
Temperature sensor	mini Cori-Flow, M14	+0...+70	±0.5	°C
Gauge pressure sensor	Sitrans P DS III, 7MF4033	-1...+15	±0.13	bar
Differential pressure sensor	Sitrans P DS III, 7MF4333	-1600...+1600	±8	mbar

The inlet and outlet temperature sensors of the test section have been separately calibrated. Its accuracy after calibration was ± 0.03 K.

3. Theoretical Models

3.1. Ammonia-water model

A steady-state mathematical model has been developed using the computer software Matlab based on momentum, heat and mass transfer phenomena for an ammonia-water mixture. The model considers heat and mass transfer between the vapor and liquid phase on the tube side, and heat transfer from the liquid phase to the water on the shell side through the tube wall. After applying finite control volume method, the absorption

process is analyzed by simultaneously solving the kinetic equations for heat and mass transfer, and conservation equations for momentum, heat and energy balances.

3.1.1. Assumptions

To simplify the model, the following assumptions are applied to the model:
(1) The whole process simulated by the mathematical model is assumed to be in steady state.
(2) The interface between vapor and liquid phases on the tube side is considered to be in thermodynamic equilibrium.
(3) Heat and mass transfer only occurs in the transversal direction of the flow.
(4) The model is 1-D, which means, properties of the working fluid are assumed to be constant with the angular coordinate and only change within the axial direction.
(5) The shell of the heat exchanger is assumed to be adiabatic, heat losses to the environment are neglected.
(6) Radiative heat transfer is neglected through the whole process.
(7) Entrance effects are neglected.

3.1.2. Mass transfer equations

Mass transfer takes place between the vapor and liquid phases, it is caused by molecular diffusion combined with convection between the bulk flows and the interface.
The mass transfer from the bulk vapor to the bulk liquid is defined as positive. Based on Fick's first law of mass transfer, the molar flux of ammonia from the bulk vapor to the interface can be determined by Eq. 1, as proposed by Bird et al. [9]:

$$J_{NH_3,v} = F_v \cdot z \cdot \ln\left(\frac{z - x_{NH_3,vi}}{z - x_{NH_3,v}}\right) \tag{1}$$

where z is defined as the ratio of ammonia molar flux to the total molar flux:

$$z = \frac{J_{NH_3}}{J} \tag{2}$$

Similarly, the molar flux of ammonia from the interface to the bulk liquid can be determined using Eq. 3.

$$J_{NH_3,l} = F_l \cdot z \cdot \ln\left(\frac{z - x_{NH_3,l}}{z - x_{NH_3,li}}\right) \tag{3}$$

The mass fluxes can be obtained when the corresponding molar flux is known:

$$G_{NH_3} = J_{NH_3} \cdot M_{NH_3} \tag{4}$$

$$G_{H_2O} = J_{NH_3} \cdot \frac{1-z}{z} \cdot M_{H_2O} \tag{5}$$

3.1.3. Pressure drop calculation

The frictional pressure drop for 2-phase flow in tube side can be estimated using the correlation from Muller-Steinhagen and Heck [10]:

$$\left(\frac{dP}{dL}\right)_{tp} = C \cdot (1-q)^{1/3} + B \tag{6}$$

where

$$C = A + 2\left(B - A\right) \cdot q \tag{7}$$

The factors A and B are the frictional pressure gradients for the liquid and the vapor phase, respectively:

$$A = f_l \cdot \frac{G^2}{2\rho_l \cdot d} \tag{8}$$

$$B = f_v \cdot \frac{G^2}{2\rho_v \cdot d} \tag{9}$$

with

$$f_l = \frac{64}{\mathrm{Re}_l}, f_v = \frac{64}{\mathrm{Re}_v} \text{ for } \mathrm{Re}_l, \mathrm{Re}_v \le 1187 \tag{10}$$

$$f_l = \frac{0.3164}{\mathrm{Re}_l^{1/4}}, f_v = \frac{0.3164}{\mathrm{Re}_v^{1/4}} \text{ for } \mathrm{Re}_l, \mathrm{Re}_v > 1187 \tag{11}$$

The frictional pressure drop for single phase flow on the shell side can be calculated by:

$$\left(\frac{dP}{dL}\right)_{cw} = f_{cw} \cdot \frac{\rho_{cw} \cdot u_{cw}^{\ 2}}{2d_H} \tag{12}$$

The effective friction factor f_{cw} is estimated to be 22 based on the study from Nefs [11].

3.1.4. Heat transfer equations

Heat transfer takes place at two main sections in the heat exchanger: between the vapor and the liquid phases in the tube, and between the liquid phase and the cooling water through the tube wall.

The heat transfer between the vapor and the liquid phases is contributed by two parts. One part is the sensible heat caused by heat convection, the other part is the heat transfer caused by mass transfer and the enthalpy difference between the vapor and the liquid phase.

The heat transfer from the bulk vapor to the cooling water is defined as positive. The heat fluxes caused by convection from the bulk vapor to the interface and from the interface to the bulk liquid are given in Eq. 13 and 14.

$$\phi_v = \alpha_v \cdot \left(T_v - T_i\right) \tag{13}$$

$$\phi_l = \alpha_l \cdot \left(T_i - T_l\right) \tag{14}$$

Heat transfer from the bulk liquid to the cooling water can be calculated using Eq. 15.

$$Q = \frac{T_l - T_{cw}}{\frac{1}{\alpha_s \cdot \pi \cdot d_{to}} + \frac{\ln\left(d_{to}/d_{ti}\right)}{2 \cdot \pi \cdot \lambda_t} + \frac{1}{\alpha_t \cdot \pi \cdot d_{ti}}} \tag{15}$$

3.1.5. Mass conservation

Since there is mass transfer between the vapor bulk and the interface, the mass balance for the bulk vapor can be expressed as:

$$\dot{m}_{v,in} = \left(G_{NH_3} + G_{H_2O}\right) \cdot dA_i + \dot{m}_{v,out} \tag{16}$$

There is no mass accumulation within the interface, thus mass balance for the interface can be expressed as:

$$J_{NH_3,v} = J_{NH_3,l} \tag{17}$$

Similar to the bulk vapor, the mass balance for the bulk liquid can be expressed as:

$$\dot{m}_{l,in} + \left(G_{NH_3} + G_{H_2O} \right) \cdot dA_i = \dot{m}_{l,out} \tag{18}$$

3.1.6. Energy conservation

The energy balance for the bulk vapor can be expressed as:

$$\dot{m}_{v,in} \cdot h_{v,in} = \left(\phi_v + G_{NH_3} \cdot \tilde{h}_{NH_3,v} + G_{H_2O} \cdot \tilde{h}_{H_2O,v} \right) \cdot dA_i + \dot{m}_{v,out} \cdot h_{v,out} \tag{19}$$

There is no energy accumulation within the interface, thus energy balance for the interface can be expressed as:

$$\phi_v + G_{NH_3} \cdot \tilde{h}_{NH_3,v} + G_{H_2O} \cdot \tilde{h}_{H_2O,v} = \phi_l + G_{NH_3} \cdot \tilde{h}_{NH_3,l} + G_{H_2O} \cdot \tilde{h}_{H_2O,l} \tag{20}$$

The energy balance for the bulk liquid can be expressed as:

$$\dot{m}_{l,in} \cdot h_{l,in} + \left(\phi_l + G_{NH_3} \cdot \tilde{h}_{NH_3,l} + G_{H_2O} \cdot \tilde{h}_{H_2O,l} \right) \cdot dA_i = Q \cdot dy + \dot{m}_{l,out} \cdot h_{l,out} \tag{21}$$

with *dy* the control volume length. The energy balance for the cooling water can be expressed as:

$$\dot{m}_{cw,in} \cdot h_{cw,in} + Q \cdot dy = \dot{m}_{cw,out} \cdot h_{cw,out} \tag{22}$$

3.2. CO_2-NH_3-H_2O model

The CO_2-NH_3-H_2O absorption model is still under development. A comparable approach to what has been discussed in the previous section will be followed. The present experimental data have been compared to the simplified Aspen Plus model introduced in [4].

4. Experimental Results and Validation

4.1. Water/water experiment

For the first experiments, demineralised water is fed into both loops to determine the shell side heat transfer coefficient. Mass flow on the tube side is fixed at 10.0 kg/hr and the shell side mass flow ranges from 2.5 to 20.0 kg/hr. Inlet temperatures on shell and tube sides are fixed at around 60 and 110°C, respectively. The experimental results are shown in Fig. 2.

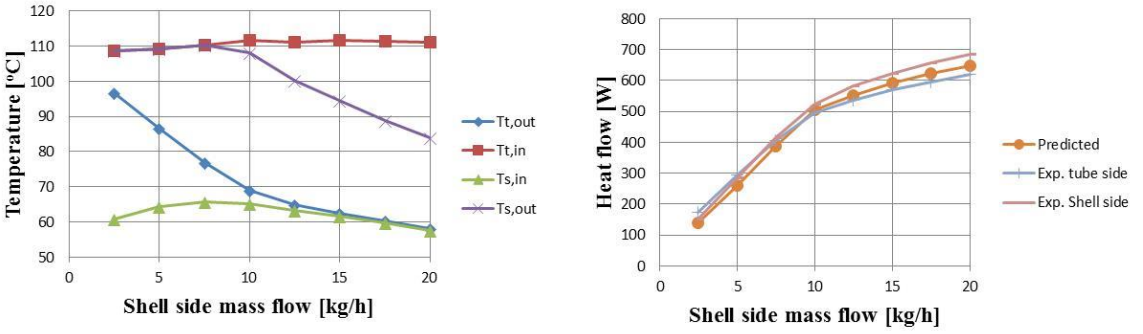

Fig. 2. Left: In- and outlet temperatures of the tube and shell side of the heat exchanger for different shell side mass flows with constant tube side mass flow (10 kg/hr); Right: Heat flow through the heat exchanger wall based on the experimental energy balances on tube and shell side and its predicted value.

The flow on both sides of the heat exchanger is laminar. There are analytical solutions for the heat transfer of single phase flow in tubes: considering constant wall heat flux (Nu = 4.364) and considering a constant wall temperature (Nu = 3.66). Both conditions do not generally apply for the experiments reported here. However for the condition in which both flows are identical (10 kg/hr) the condition of constant heat flux applies so that for that condition Nu = 4.364 must apply for the tube side. Miyatabe [12] derived analytically the Nusselt number for single phase flow along a tube bundle. Taking the discussion by Nefs [11] into account the heat transfer coefficient can be obtained from:

$$\alpha_s = \frac{\lambda_{cw}}{d_H}\sqrt{0.008495^2 + 0.4775^2 \cdot (\dot{m}_s \cdot c_{p,cw} / (\lambda_{cw} \cdot L))^{2/3}} \quad (23)$$

Where d_H is the hydraulic diameter (2.37 mm for the experimental heat exchanger). For 10 kg/hr on both sides the heat transfer coefficients become 5237 W/m^{2}K and 350 W/m^{2}K respectively for the tube and shell sides when the length, L, is taken as 0.8 m. It should be noticed that the shell side heat transfer coefficient reduces as the flow progresses along the heat exchanger. In fact a shell side heat transfer coefficient of 590 W/m^{2}K is derived from the experimental results for these conditions. Since the tube side flow has further been maintained for all experiments it can be assumed that the heat transfer coefficient on this side remains unchanged when the shell side flow is varied. This allows for the determination of the shell side heat transfer coefficient as a function of the shell side mass flow.

$$\alpha_s = 0.0001 \cdot \dot{m}_s^6 - 0.0113 \cdot \dot{m}_s^5 + 0.4056 \cdot \dot{m}_s^4 - 6.7014 \cdot \dot{m}_s^3 + 52.598 \cdot \dot{m}_s^2 - 204.43 \cdot \dot{m}_s + 1022.5 \quad (24)$$

with $\dot{m}_s$ in kg/hr and α_s in W/m^{2}K.

4.2. Ammonia-water/water experiment

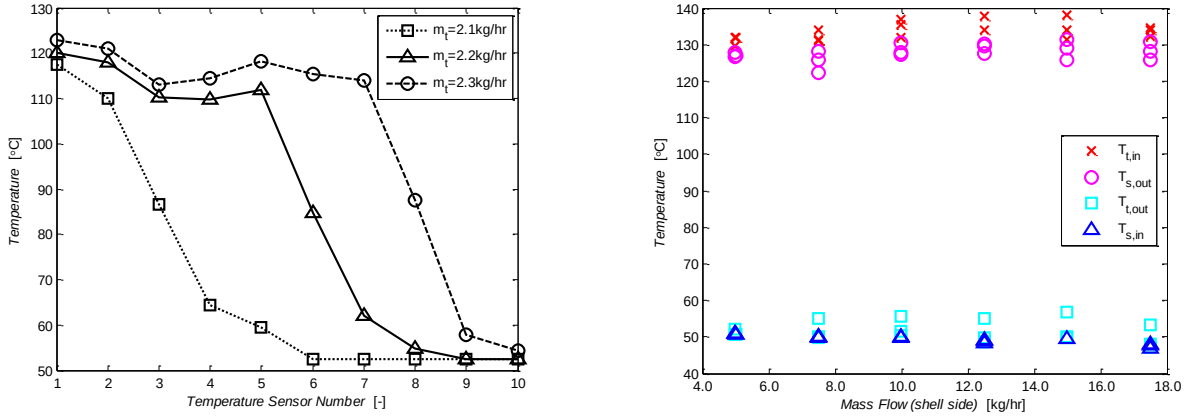

Fig. 3. Left: Shell side temperature profile when mass flow on shell side is 15 kg/hr; Right: Mini-channel heat exchanger in- and outlet temperatures as function of shell side mass flow.

De-mineralized water is replaced by ammonia-water with approximately 33.5% ammonia mass concentration in the tube side after the water/water experiments. Experiments are performed based on the principle that the tube side ammonia-water mixture is operated between slightly super-heated and slightly sub-cooled conditions. Shell side inlet temperature is fixed to approximately 50°C. Different operating conditions are obtained by changing the mass flow rate on both sides of the mini-channel heat exchanger. Mass flow on the shell side ranges from 5-17.5 kg/hr. For a fixed shell side mass flow, optimum tube side mass flow is

determined by varying its value until the heat exchange area is sufficiently used. This can be observed from the temperature profile on shell side, for example, when mass flow on the shell side is 15 kg/hr, the temperature profile corresponding to different tube side mass flows which range from 2.1 to 2.3 kg/ hr is shown in Fig. 3 (left). It can be observed that 2.2 kg/hr on the tube side is the optimum mass flow rate, while 2.1 is not sufficient and 2.3 is too high. Some of the results of the ammonia-water/water experiment are shown in Figs. 3 to 5. Notice that these ten sensors are less accurate than listed in Table 2 but clearly indicate the temperature profile trends during the experiments.

Fig. 3 (right) shows the in- and outlet temperatures of the heat exchanger for all the experiments. It reflects different operating conditions of the experiment. The principle is to fix the inlet temperatures on shell and tube side to 50 and 135 °C, respectively. Adjust the mass flow on tube side to achieve sufficient heat transfer so that the shell side outlet temperature approaches the tube side inlet temperature.

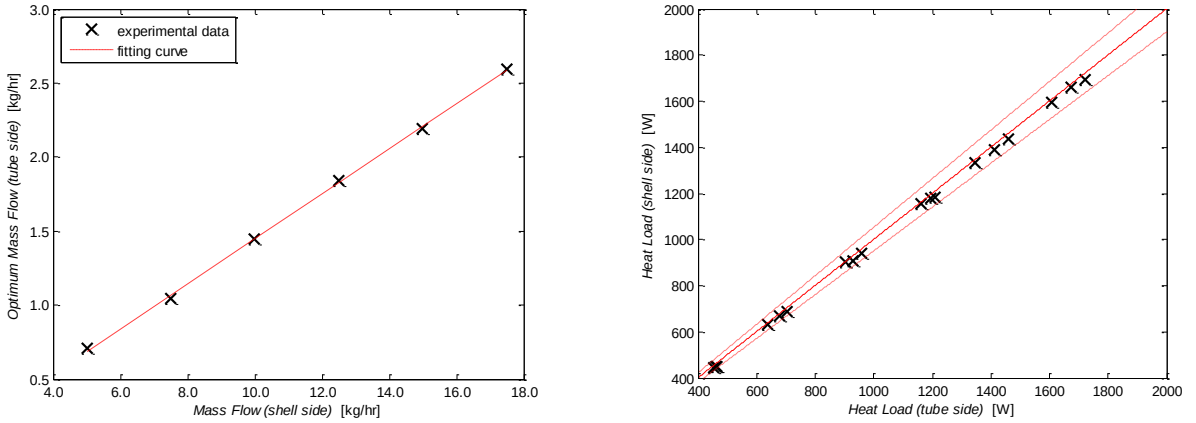

Fig. 4. Left: Optimum tube side mass flow as a function of shell side mass flow; Right: Comparison of the shell and tube side heat loads.

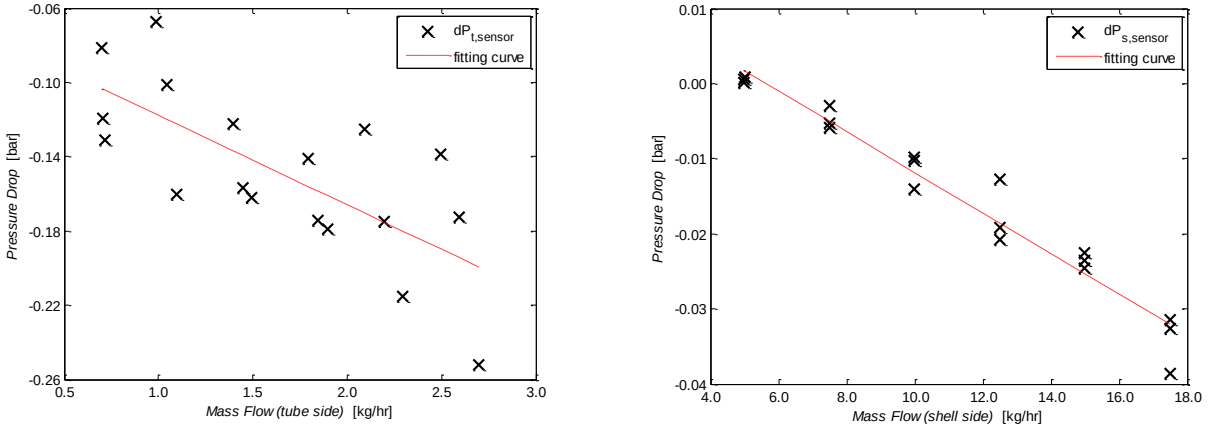

Fig. 5. Pressure drop as a function of mass flow on the tube side (left) and shell side (right)

Fig. 4 (left) shows the relation between shell side mass flow and its corresponding optimum tube side mass flow. The result gives a linear profile, the fitting curve can be expressed as:

$$\dot{m}_t = 0.1521 \cdot \dot{m}_s - 0.0708 \quad (25)$$

The heat load on both sides of the heat exchanger can be calculated by multiplying mass flows with their corresponding enthalpy differences between in- and outlet. The results from different operating conditions are shown in Fig. 4 (right). The figure shows that the tube side heat load is always slightly higher than that of the shell side. This is because of the heat transfer to the environment from the shell. The difference is within 5% (dashed lines are ± 5% error boundaries) so it can be concluded that the shell side is well insulated.

Fig. 5 shows the relation between pressure drop and mass flow on both shell and tube sides. Trends on both sides show linear profiles, although results from tube side are quite dispersed.

4.3. CO_2-NH_3-H_2O mixture/water experiment

To experimentally investigate the effect of adding CO_2, a small amount of CO_2 has been added to the tube side. For the first experiments, mass fractions of CO_2 and NH_3 are 2.1% and 32.8% respectively. Similar to ammonia-water/water experiment, inlet temperatures on shell and tube sides are fixed to around 50 and 135°C. Shell side mass flow rate ranges from 5 to 17.5 kg/hr. Comparable to ammonia-water/water experiment, tube side mass flow is adjusted until outlet temperatures on both sides are identical to those from ammonia-water/water experiment. Some of the results are shown in the following figures. These experiments have been repeated to verify its reproducibility and showed to be reproducible. This has been done because, at higher flows, the pump circulation with CO_2 added became quite unstable. This instability might be caused by un-absorbed CO_2 gas which passes the pump. If this is the case it indicates that the kinetics of the CO_2 absorption are slow which might be a problem in practical systems.

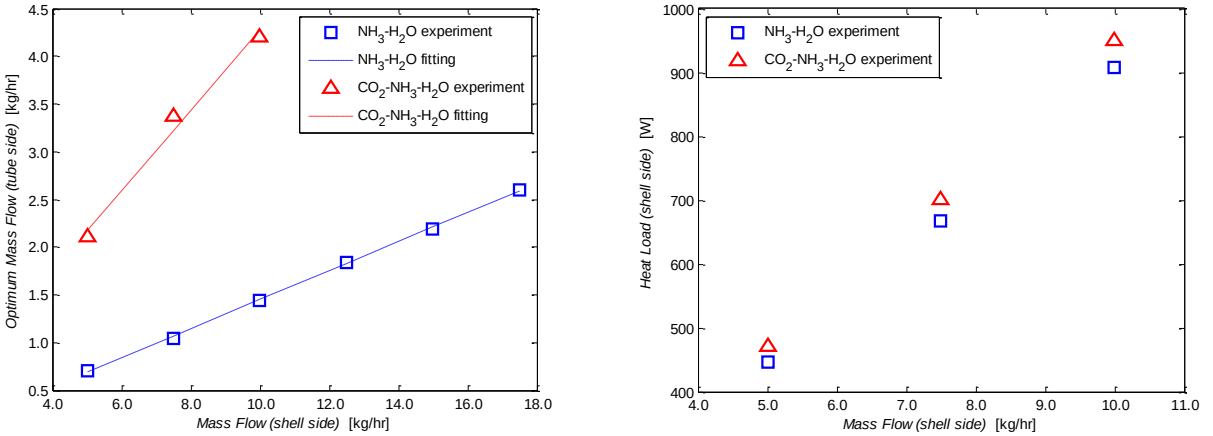

Fig. 6. Left: Comparison of optimum tube side mass flow as a function of shell side mass flow between two different working fluids; Right: Comparison of shell side heat load between the two different working fluids

The red curve shown in Fig. 6 (left) represents the relation between shell side mass flow and its corresponding optimum tube side mass flow for CO_2-NH_3-H_2O mixture/water experiment. It can be concluded that higher mass flow on tube side is needed to get comparable heat transfer rate for CO_2-NH_3-H_2O mixture compared to ammonia water. Fig. 6 (right) indicates that when reaching optimum operating conditions, CO_2-NH_3-H_2O mixture/water experiment can have as much as 5% more heat transferred.

Fig. 7 compares pressure drop on both sides between two experiments with different working fluids. Shell side pressure drop from the two experiments (left) shows great accordance with each other. Tube side pressure

drop comparison (right) indicates that CO_2-NH_3-H_2O mixture has better performance than ammonia water since it gives lower pressure drop.

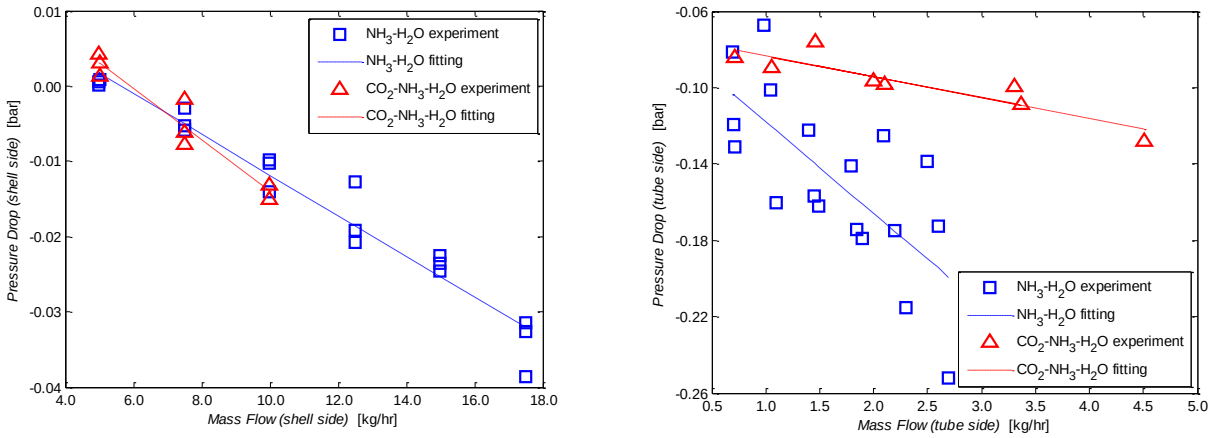

Fig. 7. Comparison of pressure drop as a function of mass flow on the shell side (left) and tube side (right) between two different working fluids

4.4.Ammonia-water model validation

Ammonia-water/water experiment results are used to validate the ammonia-water theoretical model. Tube inlet and shell outlet conditions (temperature, pressure, mass flow) are applied to the model as the inputs. Tube outlet and shell inlet conditions together with other parameters calculated from the model can be compared with the experimental data. Some of the results are shown in Fig. 8.

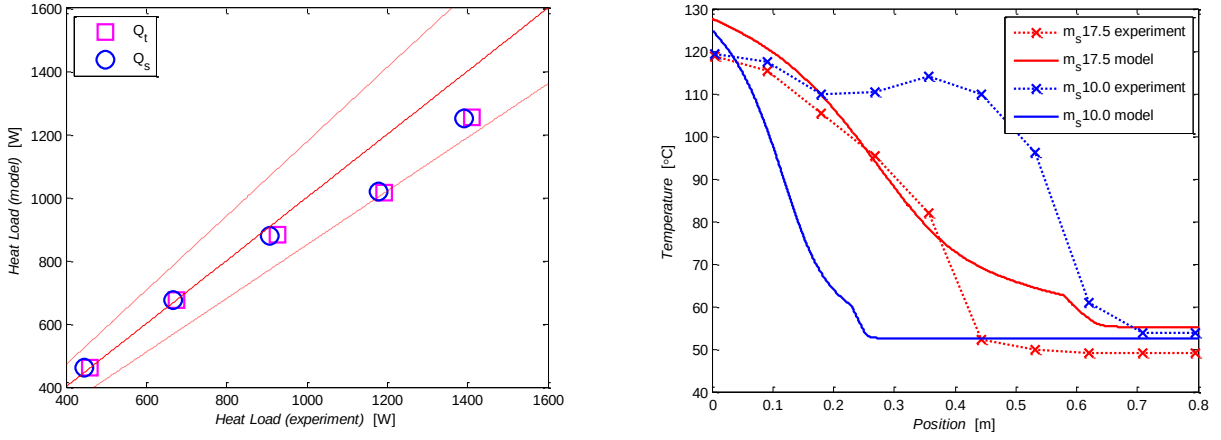

Fig. 8. Left: Shell and tube side heat load comparison between experimental data and theoretical model results; Right: Shell side temperature profile comparison between experimental data and theoretical model results

Fig. 8 (left) compares the heat load of the experimental data and of the theoretical model results on both sides of the heat exchanger. Heat loads of the experimental data are calculated by multiplying mass flows with their corresponding enthalpy differences of the fluid. The red dashed lines are the boundaries with $\pm$15% error.

It can be observed that all the data are within the boundary, the model can predict the heat load of the mini-channel heat exchanger with reasonable accuracy.

Cooling water temperature profile along the heat exchanger calculated using the theoretical model can be validated by the experimental data from the ten temperature sensors attached along the shell. Although the accuracy of these temperature sensors are low, they give an idea about how the trend would be like. Results for two different operating conditions are shown in Fig. 8 (right). It can be observed that the model has successfully predicted the shell side temperature profile, because for both cases the slopes of the curves are similar, also the effective heat exchange area predicted by the model is similar to that of the experimental data. Since the model starts calculation from the 2-phase condition, the superheated condition at the inlet of the tube cannot be predicted, this caused the interval between the blue curves.

5. Conclusions

This study is the first to investigate successfully the experimental aspects of the absorption process of a CRHP with the ternary mixture NH_3-CO_2-H_2O. A model has been developed for ammonia-water which takes into account the kinetics and mass transfer during the absorption process. The model has been validated against experiments performed for an absorption process in a mini channel heat exchanger with NH_3 concentration of 35 wt%. The results show a good match between the model and the experiments (within 15% error). Experiments have also been performed with 2.1% CO_2 weight fraction and 32.7% NH_3 which indicated a heat flow rate increase of up to 5% when CO_2 was added when compared to only ammonia-water. However it should be remarked that, with CO_2 added, the working fluid flow became unstable above 4.0 kg/h.

Acknowledgements
This is an ISPT (Institute for Sustainable Process Technology) project.

References

[1] CBS, 2006. URL: *http://statline.cbs.nl/StatWeb/publication/?DM=SLEN&PA=83140ENG&la=en*
[2] Van de Bor DM, Infante Ferreira CA, Kiss AA. Low grade waste heat recovery using heat pumps and power cycles. *Energy*. 2015;**89**: 864-873.
[3] Kiss AA, *Advanced distillation technologies - design, control and applications*. Chichester, UK: John Wiley & Sons; 2013.
[4] Gudjonsdottir V, Infante Ferreira CA. Comparison of models for calculation of the thermodynamic properties of NH_3-CO_2-H_2O mixture. International Refrigeration and Air Conditioning Conference; 2016.
[5] Van Leeuwen JM. *Absorption and desorption of ammonia-water mixtures in mini-channel heat exchangers.* Delft University of Technology. Master thesis; 2011.
[6] Fernandez-Seara J, Sieres J, Rodriguez C, Vazquez M. Ammonia-water absorption in vertical tubular absorbers. *International Journal of Thermal Sciences*. 2005; **44**: 277-288.
[7] Rijpkema J. *Experimental validation of a new ammonia/water absorption model in a minichannel annulus*. Delft University of Technology. Master thesis; 2012.
[8] Nefs CWM, Van de Bor DM, Infante Ferreira CA. Laminar single phase flow distribution in a multi-tube mini-channel heat exchanger using fractal distribution. *Chemical Engineering and Processing*.2015; **80**: 29–37.
[9] Bird RB, Stewart WE, Lightfoot EN. *Transport phenomena.* 2nd ed. New York: John Wiley & Sons; 2002.
[10] Muller-Steinhagen H, Heck K. A simple friction pressure drop correlation for two-phase flow in pipes. *Chemical Engineering and Processing: Process Intensification*. 1986; **20**: 297-308.
[11] Nefs CWM. *Experimental validation of a mini-channel multi-tube ammonia-water absorption/desorption model*. Delft University of Technology. Master thesis; 2013.
[12] Miyatake O. Laminar-flow heat transfer to a fluid flowing axially between cylinders with a uniform wall heat flux. *Int. J. Heat Mass Transfer.* 1991;**34**: 322–327.